Three-body Moon-Mars transfer with revisited weak stability boundary concept and aerobraking capture

IAC-23-78200

Three-body Moon-Mars transfer with revisited weak stability boundary concept and aerobraking capture

Gabriele Mocciola[a]*, Luigi Mascolo[b], Manuela Battipede[c]

[a] *Department of Mechanical and Aerospace Engineering, Politecnico di Torino, Corso Duca degli Abruzzi 24, Turin, Italy,* gabriele.mocciola@studenti.polito.it
[b] *Department of Mechanical and Aerospace Engineering, Politecnico di Torino, Corso Duca degli Abruzzi 24, Turin, Italy,* luigi.mascolo@polito.it
[c] *Department of Mechanical and Aerospace Engineering, Politecnico di Torino, Corso Duca degli Abruzzi 24, Turin, Italy,* Manuela.battipede@polito.it
* Corresponding Author

Abstract

In recent years, the next declared goal of the human race is landing on Martian soil and, in view of this, the roadmap to Mars envisages, as an intermediate step, the creation of a Moon Village in order to accumulate experience of extraterrestrial life, improving the technological and generation capabilities of energy sources outside our Earth.
In light of this, the study carried out within this research work tries to explore possible ways for future unmanned supply missions to the Martian soil both in preparation for subsequent human exploration and for the creation of a possible Mars Village.
Therefore, this paper presents a minimum propellant study for an interplanetary trajectory from the Moon to Mars, focusing on exploiting Weak Stability Boundary (WBS) trajectories. The mission assumptions at departure include impulsive manoeuvres, N bodies perturbation, and JPL's DE440 ephemerides for the Moon and other celestial bodies position at epoch. The payload fraction is maximized via a genetic evolution method. The escape trajectory from the Earth-Moon binary sphere of influence towards Mars is optimized by a revised WSB trajectory that includes an Earth-gravity assisted slingshot at departure. The epoch-dependent position of Mars and the cost to reach it from Earth are derived by solving the Lambert problem and by slicing isocurves at the threshold identifying solution at lower cost using WSB trajectories or traditional Earth-gravity assist strategies. The spacecraft state at the Earth-Moon sphere of influence is patched to the heliocentric leg, which evolves under Keplerian motion.
The analysis contains a study concerning the influence of solar pressure on the escape phase, with references to variations in velocity and energy, and based on the Sun-spacecraft relative position depending on the starting date.
Results clearly show that there is a significant bifurcation phenomenon between using WSB trajectories and traditional Earth-gravity assist strategies. Future studies could explore the possibility of using Deimos and Phobos gravity assists to further optimize trajectories and reduce mission costs.
Keywords: Weak Stability Boundary, escape trajectory, n-body problem, genetic algorithm, lunisolar perturbation, Moon-Mars transfer

Nomenclature

Symbol	Definition
a, **a**	Acceleration
a	Semi-major axis
dv	delta-V
e	Eccentricity
$\mathcal{E}$	Specific mechanical energy
G	Universal gravitational constant
m, m	mass
r	Radius
t	time
u, v, w	radial, tangential, normal velocity
V	Velocity
x, y, z	Cartesian coordinates
$\boldsymbol{\gamma_p}$	supplementary accelerations
θ	angle at Epoch
ϑ	declination angle
μ	Specific gravitation parameter (Earth)

Subscript	
E	Earth
i	i-th individual
ℓ	Lunar
S	Sun
SC	Spacecraft
x, y, z	respective axis

Acronyms/Abbreviations

Earth Mean Equator and Equinox of Epoch J2000	EME2000
Earth-Moon	EM
Genetic Algorithm(s)	GA(s)
International Celestial Reference Frame	ICRF
Lunar low orbit	LLO
n − Body Problem	NBP
Navigation and Ancillary Information Facility	NAIF

Planar Circular Restricted 3-Body Problem	PCR3BP
Sphere Of Influence	SOI
Weak Stability Boundary	WSB

1. Introduction

In the most fervent years of space exploration, the avowed goal of this and future generations is the human landing on Martian soil and, with it, the conquest of an extraterrestrial independence that is as much a sign of strength as it is of hope, so that a life beyond our cradle is possible.

In order for human settlement on Mars to be functional and sustainable, in addition to the realisation of manned missions to the red planet, it is necessary to envisage what resources may be required to build a living and liveable environment and optimise their interplanetary expedition: communication technologies, life-support systems, space habitats, food and energy production systems as well as surface vehicles and radiation protection technologies will be necessary.

With this in mind, and attempting to respond to this need, the present paper proposes to study a low-cost Moon-Mars transfer by exploiting and readapting the concept of Weak Stability Boundary (WSB) to the n-Body Problem (NBP).

The research work carried out and reported here has investigated, in particular detail, the phase of escape from the sphere of influence of the Earth-Moon complex from a low lunar orbit (LLO) with the aim of minimising the required delta-V.

The study carried out was organised in two phases. At first, out of a desire to better understand the WSB concept and, at the same time, to lighten the computational cost, it was decided to model the motion in the Planar Circular Restricted 3-Body Problem (PCR3BP) on which an ad hoc genetic algorithm was stitched.

The PCR3BP has been employed as the chosen model for describing the dynamics of a minute particle within the Earth-Moon system. In this particular framework, relative to an inertial reference frame, two primary celestial bodies, denoted as P_1 and P_2 with masses $m1 > m2 > 0$, respectively, execute circular orbits around their common centre of mass, influenced solely by their mutual gravitational interaction. A third body, represented as P_3(standing as the spacecraft) and regarded as having infinitesimal mass, moves within the same plane as the primaries, experiencing gravitational forces from P_1 and P_2. Importantly, the motion of this infinitesimal mass, corresponding to a spacecraft in our context, does not perturb the orbits of the primary bodies, which stand for the Earth and the Moon.

This is where the concept of WSB takes shape, i.e. a region in the phase space of a dynamical system in which orbits can be weakly stable. In this context, invariant manifolds are geometric spaces that remain unchanged under the action of a dynamical map or flow and assume importance because they can define boundaries or separations between different stability regions of the dynamical system.

The exploitation of these regions allows the design of low-energy missions.

This approach, although functional at an embryonic stage of the work and useful for carrying out a large number of simulations, proved to be incomplete.

To achieve a comprehensive and high-fidelity trajectory optimization, it becomes essential to utilize a dynamical system that closely approximates the complexities of the actual solar system. This entails accounting for all gravitational influences, perturbations, and phenomena originating from various celestial bodies within the solar system. For this purpose, we employ JPL's DE440 planetary ephemerides within the framework of the NBP dynamical system. This dynamical model encompasses the gravitational interactions of a complete-body system, consisting of the Sun, Earth, Moon, and the spacecraft itself as well as other celestial bodies in the solar system itself, while also addressing various additional perturbations and effects, which will be elaborated upon in subsequent sections.

Once the physical model, CR3BP or NBP as it may be, the trajectory search was carried out using a Genetic Algorithm (GA) stitched onto the model itself and based on a merit function that would naturally direct evolution towards the desired results.

Within the GA, the different candidates are represented as combinations of four different genes that, randomly shuffled together, lead to the creation of a pilot population (first generation) from whose evolution subsequent generations will be born.

Using offspring, ex novo generation, more or less forced mutation, crossover and recombination operators and exclusion of individuals deemed unsuitable, the mass of candidates evolves towards compliance with the imposed figures of merit.

The GA assumed a pivotal role in our study, facilitating the generation of diverse yet comparable outcomes. This approach enabled us to conduct a comprehensive analysis, not only of individual solutions but also of the broader spectrum of potential trajectories stemming from a shared initial concept. Our emphasis extended beyond singular trajectories, encompassing a collective exploration of different trajectories, all originating from the same fundamental concept. This approach afforded a valuable opportunity for critical evaluation and comparison.

As elaborated upon in the subsequent section dedicated to results and analysis, this study has unveiled the potential for executing escape manoeuvres from the sphere of influence of the Earth-Moon system, originating from low lunar orbits. This manoeuvre leverages a gravitational interdiction zone and entails a

delta-V expenditure of approximately 400 m/s enabling a ballistic escape manoeuvre.

2. Dynamical models

In the course of this investigation, diverse dynamical models are utilized to provide distinct perspectives on the spacecraft and the forces influencing it.

Within the framework of the PCR3BP, the spacecraft is treated as a point mass, subject exclusively to gravitational forces attributable to the presence of the Earth and Moon, as dictated by a static, time-independent physical model.

Conversely, when implementing the HPOP, the complete NBP is employed. This comprehensive approach considers the gravitational influences exerted by all celestial bodies within the solar system and tracks their temporal positions. Simultaneously, specific geometry (volume and wetted surface) is attributed to the spacecraft, proving instrumental in quantifying the magnitude of certain perturbative effects.

This approach enables the execution of a thorough analysis.

2.1 The planar circular restricted three-body problem

The model employed to depict the movement of an infinitesimal particle within the Earth-Moon system is known as the PCRTBP.

In this model, with reference to [1-2], concerning an inertial reference frame, two principal bodies, denoted as P_1 and P_2 with masses $m_1 > m_2 > 0$, respectively, traverse circular orbits under the influence of their mutual gravitational attraction, revolving around their shared center of mass. Meanwhile, a third body, denoted as P_3 and assumed to possess infinitesimal mass, follows a trajectory influenced by the gravitational forces exerted by the primary bodies within the same orbital plane.

Notably, the motion of the primary bodies remains unaffected by the presence of the infinitesimal mass. In our specific context, P_3 represents a spacecraft, while P_1 and P_2 correspond to the Earth and the Moon, respectively. We denote the mass ratio of the smaller body to the total mass as $\mu = m_2/(m_1 + m_2)$.

The movement of the infinitesimal mass is depicted within a co-rotating coordinate system *(x, y)*, with the origin situated at the center of mass of the two primary bodies. In this framework, we employ normalized units for distance, mass, and time. The equations governing this motion are as follows:

$$\ddot{x} - 2\dot{y} = \frac{\partial \Omega}{\partial x}, \qquad \ddot{y} - 2\dot{x} = \frac{\partial \Omega}{\partial y}, \tag{2.1}$$

where the effective potential Ω is given by

$$\Omega(x,y) = \frac{1}{2}(x^2 + y^2) + \frac{1-\mu}{r_1} + \frac{\mu}{r_2} + \frac{1}{2}\mu(1-\mu),$$

with $r_1 = ((x+\mu)^2 + y^2)^{1/2}$, $r_2 = ((x+\mu-1)^2 + y^2)^{1/2}$ as P_1, P_2 are located at $(-\mu, 0)$, $(1-\mu, 0)$, respectively.

The dynamics represented by equation (2.1) exhibit five equilibrium points denoted as L_k, where $k = \{1, 2, \ldots, 5\}$, commonly referred to as the Euler–Lagrange libration points. Three of these equilibrium points, namely L_1, L_2, and L_3, are situated along the x-axis.

In the current notation, L_1 is positioned between the Earth and the Moon, while L_2 lies beyond the Moon.

The remaining two points, L_4 and L_5, are located at the vertices of two equilateral triangles, both sharing a common base extending from P_1 to P_2.

The set of differential equations (2.1) possesses a conserved quantity known as the Jacobi integral

$$J(x, y, \dot{x}, \dot{y}) = 2\Omega(x, y) - (\dot{x}^2 + \dot{y}^2)$$

The mapping of an energy manifold onto the configuration space *(x, y)* is referred to as a Hill's region. The trajectory of P_3 remains consistently within the Hill's region associated with the specific Jacobi energy denoted as C. The boundary of a Hill's region corresponds to a zero-velocity curve. Notably, the Hill regions undergo changes corresponding to variations in the Jacobi energy C.

The equations represented by (2.1) can be expressed using polar coordinates *(r, θ)* relative to P_2. Here, *'r'* denotes the distance from P_2 to P_3, and *'θ'* represents the angle measured counterclockwise between the axis P_1P_2 and P_2P_3.

If the trajectory of P_3 commences from the periapsis ($\dot{r} = 0$) of an osculating ellipse revolving around the Moon, characterized by a semi-major axis *'a'* and an eccentricity *'e'* falling within the range *[0, 1)*, and it possesses an initial velocity *'v'* concerning the sidereal reference frame, then the following relations apply:

$$r = a(1-e), \qquad V = \sqrt{\frac{(1+e)\mu}{r}} \tag{2.2}$$

In the definition of the WSB, we will need to refer to the Kepler energy $\mathcal{E}_2$ of P_3 with respect to the the primary P_2. This is given by

$$\mathcal{E}_2 = \frac{1}{2}V^2 - \frac{\mu}{r}$$

Considering the (2.2), it follows

$$\mathcal{E}_2 = \frac{(e-1)\mu}{2r}$$

2.1.1 Weak Stability Boundary definition

We examine trajectories that originate from a radial line denoted as *'l(θ)'* and commence at point P_2, forming an angle *'θ'* with the x-axis. These trajectories are assumed to initiate from the periapsis of an osculating ellipse centered around P_2, where the semi-major axis *'a'* of the ellipse lies along *'l(θ)'* and possesses a fixed eccentricity *'e'*, resulting in a value of $r_2 = a(1-e)$. The initial velocity of the trajectory is directed perpendicular to *'l(θ)'*, and the Keplerian energy of P_3 concerning P_2 is represented as *'* $\mathcal{E}_2$*'* with $\mathcal{E}_2 < 0$. It's worth noting that in this definition, $\dot{r} = 0$.

The trajectory, when *'θ'* and *'e'* are held constant, solely depends on the distance r_2. We classify the motion as *'stable'* when, subsequent to departing from *'l(θ)'*, P_3 completes a full orbit around P_2 without encircling P_1 and eventually returns to *'l(θ)'* at a point where $\mathcal{E}_2 < 0$. Conversely, if this condition is not met, the motion is referred to as *'unstable'*.

Starting from this juncture, it becomes intriguing to assess the behaviour of P_3 as it ventures into the WSB or a comparable gravity-bound region, where the influence of other celestial bodies starts to play a role. In this context, it proves advantageous to introduce the concept of ballistic escape [3].

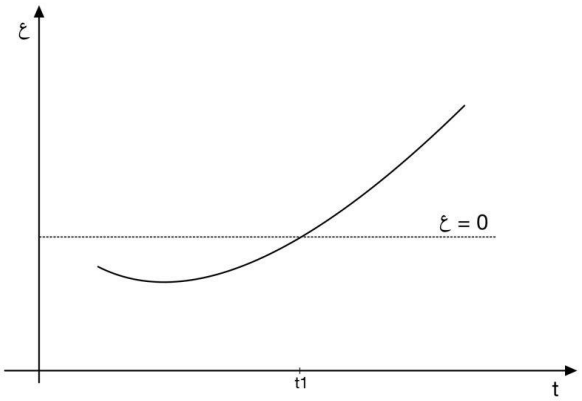

P_3 undergoes ballistic ejection (or ballistically escapes) from P_2, following the trajectory defined by ψ(t), at a specific time denoted as *'t_1'* if

$$\mathcal{E}_2\big(\psi(t)\big) < 0, \qquad \text{for} \quad t < t_1$$

and

$$\mathcal{E}_2\big(\psi(t)\big) \geq 0, \qquad \text{for} \quad t \geq t_1.$$

2.2 High Precision Orbit Propagator and N-body problem

This propagator serves as a powerful tool for studying escape manoeuvres from EM's sphere of influence within the N-body model. By considering a wide array of perturbing forces and employing advanced numerical integration techniques, it provides valuable insights into the dynamics of such manoeuvres and their feasibility in the complex gravitational environment of the solar system.

In our pursuit of analyzing a satellite's escape trajectory from the sphere of influence of Earth and the Moon within an NBP, we find ourselves navigating a complex interplay of forces governing the satellite's motion. Foremost among these forces is Earth's central gravity, which serves as the cornerstone of our motion model. However, to faithfully capture the intricacies of the satellite's perturbed motion, a meticulous consideration of numerous perturbations becomes imperative, a categorization that neatly divides into gravitational and non-gravitational forces.

The resultant equation of motion, with reference to [4], can be compactly expressed as:

$$\ddot{\boldsymbol{r}} = -\frac{GM}{r^3}\boldsymbol{r} + \boldsymbol{\gamma_p}$$

Here, $\boldsymbol{\gamma_p}$ emerges as the vector encompassing supplementary accelerations, a set of influences resulting from perturbing forces. These additional accelerations encompass:

i. *Non-Spherical and Inhomogeneous Mass Distribution within Earth(* $\ddot{r}_E$ *)*: This intricate dance of accelerations arises from Earth's mass distribution, which deviates from sphericity and uniformity. This deviation finds its origins in Earth's varied terrain and the density distribution lurking beneath its surface.

ii. *Gravitational Forces from Celestial Bodies(*$\ddot{r}_S$, $\ddot{r}_M$, $\ddot{r}_P$ *)*: Beyond Earth's gravitational grasp, celestial companions such as the Sun, Moon, and planets join the motion. Each celestial body contributes its gravitational pull, casting its unique accelerative spell upon the satellite.

iii. *Terrestrial and Oceanic Tide Effects(*$\ddot{r}_e$, $\ddot{r}_o$ *)*: The perpetual ebb and flow of terrestrial and oceanic tides, choreographed by the gravitational forces of the Moon and the Sun, usher in their own distinctive accelerations. These tidal forces affect both Earth and the satellite in their cosmic trip.

iv. *Atmospheric Drag(*$\ddot{r}_D$*)*: As the satellite journeys through Earth's atmosphere, it encounters resistance, instigating accelerations due to atmospheric drag. The density of the atmosphere and the satellite's velocity wield considerable influence in shaping these accelerations.

v. *Solar Radiation Pressure(*$\ddot{r}_{SP}$, $\ddot{r}_A$*)*: The radiant pressure exerted by sunlight, whether directly or reflected, introduces additional accelerations into the equation. These accelerations arise from

the exchange of momentum between the satellite's surface and the incoming photons. Factors such as the satellite's reflectivity and geometry play pivotal roles in determining the extent of these accelerations.

vi. *Unmodeled Forces($\ddot{r}_{emp}$)*: The realm of unmodeled forces represents a frontier of perturbations stemming from various sources not explicitly accounted for. These forces may include subtle gravitational interactions with smaller celestial bodies or localized variations in Earth's gravitational field.

In the specific scenario under investigation, as our simulations progressed, a notable observation came to the forefront: the term associated with tidal influences could be safely neglected, offering a modest yet noteworthy computational simplification.

The tide-induced forces, while undoubtedly a captivating aspect of celestial mechanics, emerged as a relatively minor contributor within the broader context of our simulation. Their impact, though intriguing, paled in comparison to the dominant forces steering the satellite's motion, such as central gravity, gravitational effects from celestial bodies, atmospheric drag, and solar radiation pressure.

This realization opened a path towards a more streamlined computational approach. By judiciously excluding the tidal term from our calculations, we achieved a welcome reduction in computational overhead, thereby enhancing the efficiency and expediency of our simulations. This strategic decision, founded on rigorous analysis and scientific pragmatism, allowed us to allocate computational resources more judiciously and focus our efforts on the primary drivers of the satellite's dynamic behavior.

In the ever-evolving landscape of scientific inquiry and numerical modeling, such discerning choices are integral to achieving a balance between precision and computational efficiency. The nuanced understanding gained from this strategic simplification underscores the importance of adaptability and optimization in the pursuit of scientific exploration.

To embark on the faithful simulation of the satellite's perturbed motion, we harnessed the prowess of a Runge-Kutta-Fehlberg integrator. This computational juggernaut was seamlessly integrated with a comprehensive force model, a virtual toolkit spanning:

- The gravitational field of Earth, meticulously represented through the GGM03C model.
- The gravitational influences of planets within our solar system, their positions meticulously computed via the JPLDE440 dataset.
- The nuanced effects of atmospheric drag, which gracefully accommodates various atmospheric density models for utmost fidelity.
- The intricate dance of solar radiation pressure, artistically interpreted through conical, geometrical, or cylindrical shadow models.
- The inclusion of solid Earth tides, as dictated by the IERS Conventions of 2010.
- The harmonious influence of ocean tides.
- The indomitable force of general relativity, a pillar of accuracy in the simulation.

In summation, this comprehensive and meticulously articulated framework serves as a potent instrument in our endeavour to unravel the escape trajectory of a satellite from the gravitational embrace of Earth and the Moon within the context of the N-body problem. By embracing both gravitational and non-gravitational forces, our model offers a panoramic view of satellite dynamics in the exquisitely complex gravitational theatre of our solar system.

2.2.1 Influence of the fourth body

As extensively highlighted in [5-6], throughout the escape trajectory, the Sun undergoes apparent motion relative to the Earth, observed within the EME2000 reference frame.

This motion introduces a time-varying perturbation that has significant implications for the trajectory. Under certain simplifying assumptions, this perturbation generates a cumulative perturbing acceleration acting along the radial and tangential directions.

These perturbing accelerations are quantitatively described by equations for the sake of clarity and precision.

$$\left(\mathbf{a}_{SC_S} - \mathbf{a}_{E_S}\right) \cdot \hat{\boldsymbol{u}} = \frac{3}{2}\frac{\mu_S}{r_{E_S}^3}\{1 + cos[2(\vartheta_S - \vartheta)]\}.$$

$$\left(\mathbf{a}_{SC_S} - \mathbf{a}_{E_S}\right) \cdot \hat{\boldsymbol{v}} = \frac{3}{2}\frac{\mu_S}{r_{E_S}^3} sin[2(\vartheta_S - \vartheta)].$$

Equations and show that it is possible to enclose the perturbation effect dependence on the Sun-spacecraft position in two proportionality terms

$$\sigma_u = 1 + \cos(2\Delta\vartheta),$$

$$\sigma_v = \sin(2\Delta\vartheta),$$

where $\Delta\vartheta$ is the angular difference between the Sun and the spacecraft.

3. Reference system

In the scope of this paper, as clearly explained in [5], the geocentric-equatorial reference system (RS) aligns precisely with the Earth Mean Equator and Equinox of Epoch J2000 (EME2000). The analysis leverages JPL ephemerides from the DE4xx series, with a specific focus on the JPL DE440 dataset. Notably, these ephemerides

are referenced in the International Celestial Reference Frame (ICRF) and encompass nutational and librational phenomena.

Historically, these intrinsic wobbling effects have conferred upon the EME2000 reference frame, also recognized as J2000, a quasi-inertial characterization. However, it is essential to acknowledge that the rotational offset between the ICRF and the dynamical EME2000 amounts to a mere hundredth of an arcsecond. Consequently, the EME2000 reference frame is now unequivocally regarded as inertial.

4. Porkchop-plot analysis

As clarified in [7], the Porkchop plots are clear and straightforward graphical tools that assist mission designers in carefully planning the most convenient dates for scheduling a transfer between two celestial bodies. These charts consist of contour curves that can represent the value of various parameters as a function of the departure date and arrival date. One of the key parameters for determining the feasibility of a mission is the total transfer cost ΔV, in terms of the velocity difference required to perform the necessary maneuvers.

In addition to aiding in the selection of optimal launch and arrival windows, Porkchop plots play a critical role in solving Lambert's problem, which is essential for precise trajectory planning. Lambert's problem involves determining the Keplerian orbital parameters (semi-major axis, eccentricity, and true anomaly) for the initial and final orbits of a spacecraft undergoing a transfer between two points in space. This problem is closely tied to the concept of ΔV optimization, as it directly impacts the fuel efficiency and overall success of the mission.

By integrating the principles of Lambert's problem within Porkchop plots, mission designers can not only identify favorable transfer windows but also fine-tune trajectory parameters to minimize ΔV requirements. This integration enhances the precision and efficiency of interplanetary mission planning, ensuring that missions are executed with the utmost accuracy while minimizing fuel consumption and associated costs.

Cognizant of our specific mission requirements, a strategic approach was adopted, necessitating the utilization of three distinct Porkchop plots.

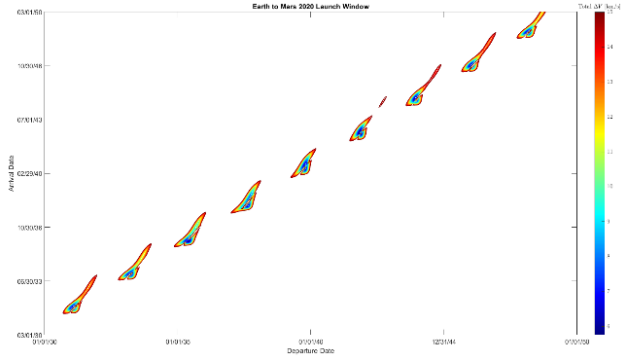

The first plot, spanning 2030 to 2050, served as the foundation for our trajectory assessment, catering to the imperative of comprehensive temporal coverage.

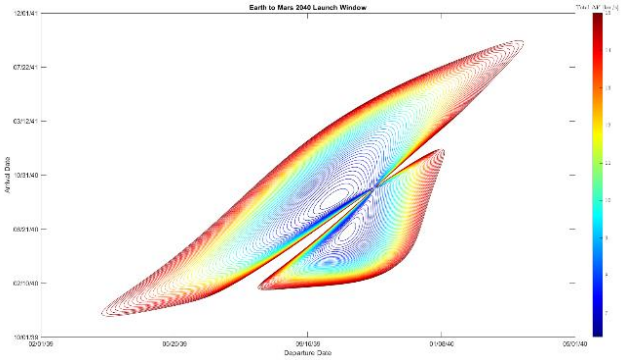

The second plot, a focused endeavour to identify the absolute minima within the Porkchop family, was essential for pinpointing optimal transfer windows. This meticulous approach allowed us to identify the most cost-effective and energetically efficient solutions, thereby reducing ΔV requirements and mission cost.

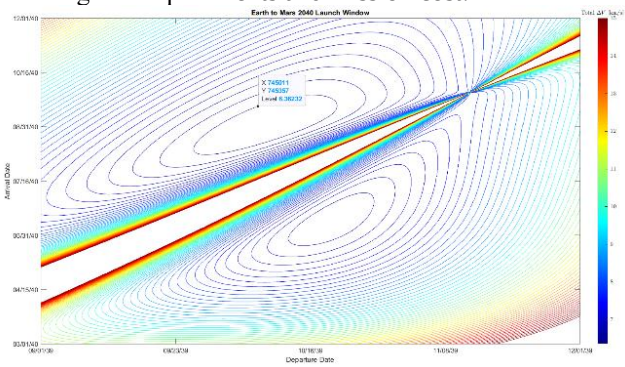

Lastly, the tertiary plot was systematically devised to afford enhanced legibility and nuanced insight into the spectrum of departure dates that held paramount interest.

In synthesizing these three Porkchop plots, we have effectively harnessed the power of graphical analysis, guided by Lambert's problem resolution principles, to refine our analysis planning and to optimize the GA's input parameters.

5. Genetic Algorithm

In the context of analyzing space trajectories and escape maneuvers from Earth and Moon's sphere of influence in an N-body problem, the design and optimization of such trajectories represent a crucial challenge. The inherent complexity of these problems calls for advanced computational methods to effectively explore the solution space.

Among various optimization approaches, Genetic Algorithms (GAs) emerge as a powerful tool to tackle the intricacies of space trajectories. As explained in [8], GAs draw inspiration from the evolutionary mechanisms of nature, replicating the process of natural selection to generate optimal or near-optimal solutions. These

algorithms are particularly well-suited for problems where the solution space is vast and intricate, as is the case with space escape maneuvers.

In this study, a Genetic Algorithm specifically designed for optimizing space escape trajectories is presented. The GA plays a pivotal role in our research approach, enabling the exploration of a wide range of parameters and efficiently generating high-quality solutions.

In this article, a detailed description of written GA will be provide, elucidating its key components and fundamental principles. We will also examine how the GA has been applied to the specific space escape trajectories considered in this research. The goal is to offer a clear understanding of the crucial role played by the GA in optimizing space trajectories and how it contributes to the significant results achieved in the context of our investigation.

5.1 Initial conditions

Though not an explicit component of the fitness calculation or the central evolutionary algorithm, the meticulous construction of initial conditions assumes a fundamental role within the framework of the algorithm under scrutiny. This phase represents the critical foundation upon which subsequent trajectory optimization endeavors are built. Leveraging the formidable capabilities of NASA's SPICE toolkit from NAIF and employing the requisite kernel data, we are able to extract precise state vectors corresponding to key celestial bodies, prominently including the Moon. Moreover, as will be expounded upon in subsequent sections, this extends to encompass the Sun and Earth.

In tandem with the initial conditions extraction, the establishment of the population, while initially generated entirely from scratch at the onset of the algorithm, assumes a significant role. This process adheres to a set of meticulously defined constraints, informed by the outcomes of prior research within the context of the Three-Body Problem within the PCR3BP. Notably, these constraints are strategically designed to ensure that the initial population adheres to mission-specific requirements. One such requirement is the imposition of a delta-V budget, thoughtfully bounded within the range of 300 to 600 meters per second. This budget not only reflects mission constraints but also trajectory optimization process towards achieving the desired objectives.

Now, the initial conditions have been computed as follows:

$$\begin{cases} x_{0,i} = x_\ell + h_0 \cdot \cos(\theta_i + \theta_\ell) \cdot \cos(\varphi_i + \varphi_\ell) \\ y_{0,i} = y_\ell + h_0 \cdot \sin(\theta_i + \theta_\ell) \cdot \cos(\varphi_i + \varphi_\ell) \\ z_{0,i} = z_\ell + h_0 \cdot \sin(\varphi_i + \varphi_\ell) \\ u_{0,i} = u_\ell + V_C \cdot \cos(\theta_i + \theta_\ell + 90°) \cdot \cos(\varphi_i + \varphi_\ell) \\ v_{0,i} = v_\ell + V_C \cdot \sin(\theta_i + \theta_\ell + 90°) \cdot \cos(\varphi_i + \varphi_\ell) \\ w_{0,i} = w_\ell + V_C \cdot \sin(\varphi_i + \varphi_\ell) \end{cases}$$

$$\begin{cases} dv_{x,i} = \Delta V_i \cdot \cos(\theta_i + \theta_\ell + 90°) \cdot \cos(\varphi_i + \varphi_\ell) \\ dv_{y,i} = \Delta V_i \cdot \sin(\theta_i + \theta_\ell + 90°) \cdot \cos(\varphi_i + \varphi_\ell) \\ dv_{z,i} = \Delta V_i \cdot \sin(\varphi_i + \varphi_\ell) \end{cases}$$

$$c_{ini} = \begin{Bmatrix} x_{0,i} \\ y_{0,i} \\ z_{0,i} \\ u_{0,i} \\ v_{0,i} \\ w_{0,i} \end{Bmatrix} + \begin{Bmatrix} 0 \\ 0 \\ 0 \\ dv_{x,i} \\ dv_{y,i} \\ dv_{z,i} \end{Bmatrix}$$

.

5.2 Fitness function

The fitness function designed for the adopted genetic algorithm represents the core of the genetic selection process.

It operates on the propagation dataset (a matrix of state vectors) obtained through the integration of initial conditions suitably modified by the algorithm's individual members, expressed in terms of delta-V and angles (the first three genotypes), over a time span defined by the fourth gene of the chromosome.

The fitness function extracts three critical components from this dataset: the position vector and velocity at the 'local' first apogee, aiming to have it within the EM external WSB, and, simultaneously, the position vector at the final state, with the expectation that it extends beyond the limits of the SOI approximation.

The evaluation of the quality of each individual in the genetic algorithm is accomplished through the comparison of these three extracted quantities with their respective target values, as follows:

1. *Local Apogee 1 and 2*: The position vector of the local apogee is expected to be at a distance of 1.45e+06 km from the primary gravitational source(it aims to secure an orbit within the WSB), with a velocity of 0 m/s, corresponding to the ideal value.
2. *Final Position*: The position vector at the final state should extend beyond the boundaries of the Sphere of Influence, which is assumed to be 1.5e+06 km, and should be at least 1.3 times the radius of the SOI itself (a heuristic value, yet with the vital criterion of being 'beyond').

To facilitate the evaluation process, in addition to the total error, which is the sum of the errors related to the

above-mentioned quantities, normalized into a unified metric, individual errors for each of these quantities are also provided.

In summary, the fitness function is tasked with determining the adequacy of the solutions proposed by individuals within the genetic algorithm, ensuring they meet the necessary conditions for the desired orbit, thereby contributing to the optimization of space trajectory planning.

5.3 Evolution core

The actual evolutionary chain initiates its course downstream of the fitness function by extracting the provided outputs. Through the analysis of these outputs, it becomes possible to discern individuals that best fit the defined criteria, thus steering the progression of evolution accordingly among preserved, discarded, and newly generated individuals.

As a fundamental step in our optimization algorithm, the initial focus is on error analysis for each individual within the population. This crucial phase allows us to assess the overall quality of each solution in the context of our problem domain. Through intra-generational comparisons, we establish a hierarchical order of individuals based on their fitness performance, effectively segregating them into different tiers. At the apex of this hierarchy lies the class of elite chromosomes, which constitutes 30% of the population. These elite individuals are deemed to possess solutions of exceptional quality and are set aside to be preserved without alteration during the generational transition.

The subsequent stages of the algorithm rely on the creation of multiple stochastic 'dice' (specifically, seven) to govern key evolutionary processes: reproduction, crossover, and mutation. One critical aspect we consider is the adaptation of mutation probabilities. To encourage diversity and prevent premature convergence, mutation probabilities are designed to increase as the absence of beneficial mutations extends, thus promoting exploration in the search space.

The reproductive phase introduces an array of strategies. Individuals can be selected for reproduction based on various criteria, including:

1. *Mean-Based Reproduction*: In this strategy, one or more genes of the offspring assume the mean value of their corresponding parental genes. This approach promotes convergence toward the central values within the population.
2. *Overlap-Based Reproduction*: Here, the offspring chromosome inherits segments from both parents, fostering the recombination of advantageous gene combinations.
3. *Similarity-Based Reproduction*: In this scenario, one or more genes of the offspring take on values that lie within the range defined by the parental values, encouraging the preservation of traits within certain bounds.

Following these processes, the remaining 40% of the population is generated anew, adhering to the constraints imposed on the genetic structure. An additional layer of algorithmic efficiency is introduced through a de-duplication check, ensuring that no two identical individuals exist within the population. In cases where duplicates are detected, a forced mutation is applied, either guided by specific knowledge or implemented as a stochastic perturbation to diversify the genetic pool.

This multi-tiered approach to evolutionary optimization combines meticulous error analysis, adaptive mutation strategies, and diverse reproductive mechanisms to efficiently explore and exploit the solution space, ultimately driving the algorithm towards the discovery of high-quality solutions.

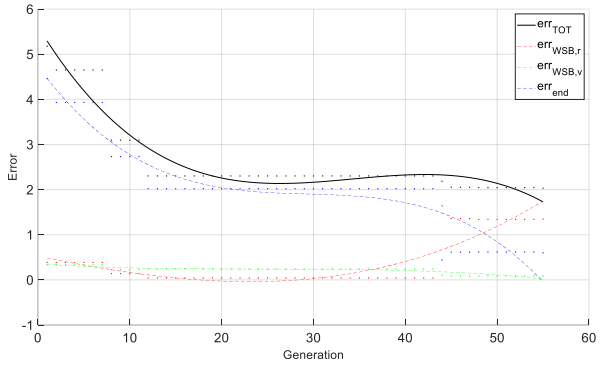

Referring to the above figure, the plot depicts the error trends across generations. In this context, we are specifically referring to the error associated with the individual that best conforms to the imposed standards. As also discernible through the interpolating polynomial of degree 3, the evolutionary trend exhibits a nearly constant generational improvement. Towards the culmination of this process, it becomes feasible to extract a defined number of elite chromosomes.

The presented figure encapsulates the essence of our optimization procedure, showcasing the continuous refinement of solutions over successive generations. The iterative nature of our algorithm facilitates the progression towards increasingly optimal solutions. It is noteworthy that the utilization of least squares approximation further underscores the robustness of this evolutionary process by demonstrating a statistically significant improvement trend.

Ultimately, upon completion of the evolutionary process, a well-defined subset of elite chromosomes can be extracted. These elite individuals represent the culmination of the algorithm's efforts, embodying solutions that best align with the predefined standards and criteria while not tying evolution to results decided a priori.

5.4 Extraction of elitists

In this context, aligning with the philosophy of a genetic algorithm that aims to explore a vast field of potentially valuable solutions, the decision has been made not to extract a single elitist individual but, rather, the top six individuals. This choice is driven by the pursuit of a more comprehensive overview of the available solution space.

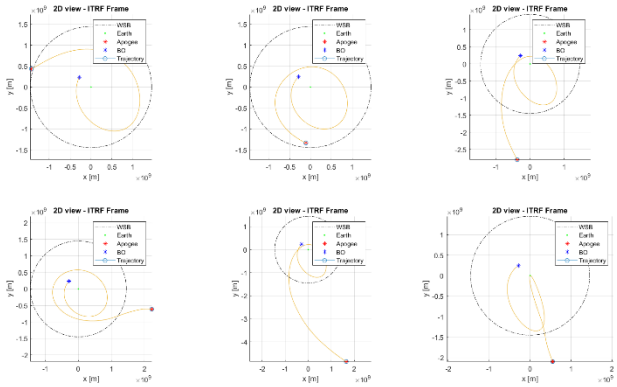

The above figure aptly demonstrates the inherent diversity in escape possibilities (which, as we shall delve into further, exhibit even greater variability). Simultaneously, it sheds light on the WSB as a region characterized by 'gravitational uncertainty.' Within this domain, the influence of the fourth celestial body (primarily, but not exclusively) emerges as a critical factor.

6. Results and discussion

In this section, we will present and analyse two distinct trajectory results, each characterized by the presence or absence of a gravity assist section.

5.4 Ballistic escape with gravity-assist trajectory

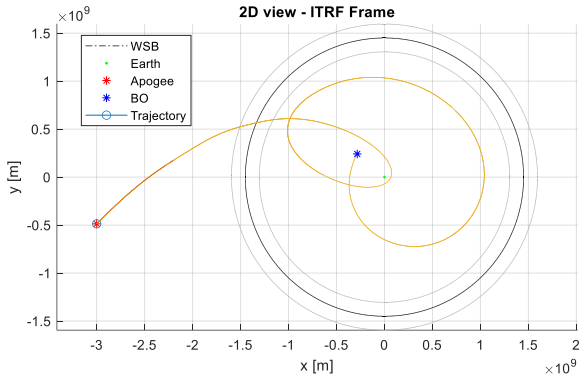

The trajectory presented here was achieved through a simulation involving a propulsion manoeuvre of 426.5m/s on September 15, 2039. The transfer duration is about 230 days.

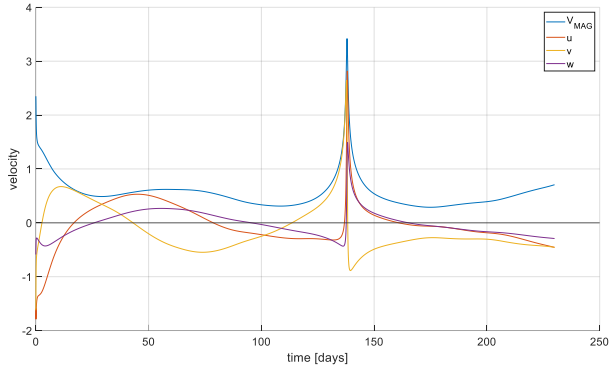

The algorithm naturally evolved towards a configuration that incorporated a gravity assist, resulting in a notable peak in velocity.

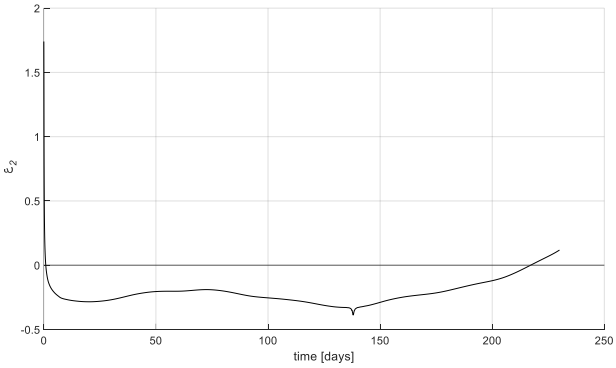

As evident from the above graph, the energy profile closely aligns with that of a ballistic escape trajectory, characterized by a change in sign of the energy parameter H_2. The oscillatory pattern observed is primarily attributed to the gravitational influence exerted by the fourth celestial body, which, in this context, is the Sun.

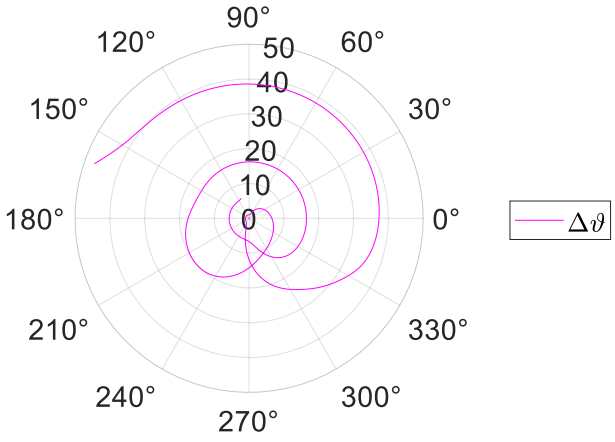

In our specific trajectory, the Sun's gravitational field emerges as the dominant influencing factor. The Sun's

gravitational perturbations induce significant variations in the spacecraft's trajectory and energy state over time, giving rise to the observed oscillations.

With reference to Section 2.2.1, the polar plot graphically illustrates the gravitational influence of the Sun on the spacecraft's trajectory. Angularly, the plot depicts the relative position of the Sun-Spacecraft system, while radially, it signifies the spacecraft's distance from the central body (in this case, Earth) within a quasi-synodic reference frame.

This representation serves as a valuable visualization tool, offering insights into the interplay between the Sun, the spacecraft, and Earth. Angularly, it showcases the dynamic positioning of the Sun relative to the spacecraft as it evolves along its trajectory. This angular information is essential for understanding the timing and magnitude of gravitational perturbations exerted by the Sun.

On the radial dimension, the plot conveys the varying distance of the spacecraft from the central body, Earth. This information is pivotal in assessing the changing gravitational forces acting on the spacecraft as it traverses its trajectory. It allows us to quantify the impact of the Sun's gravitational pull in relation to the spacecraft's position within the quasi-synodic reference frame.

By combining both angular and radial data, this polar plot provides a comprehensive view of the complex gravitational dynamics experienced by the spacecraft. It aids in discerning patterns, eventual periodicities, and key events that are crucial for mission analysis and trajectory optimization.

5.4 Ballistic escape without gravity-assist trajectory

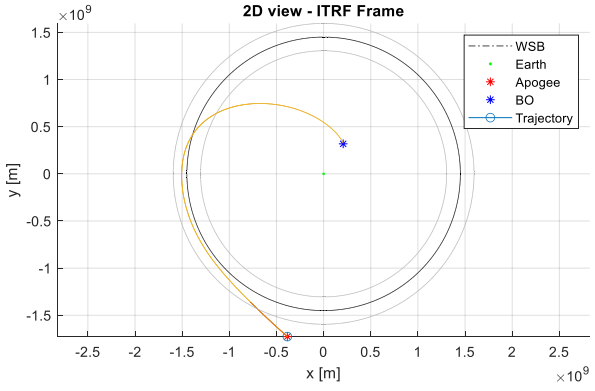

The trajectory presented here was achieved through a simulation involving a propulsion manoeuvre of 471m/s on October 06, 2039. The transfer duration is about 90 days.

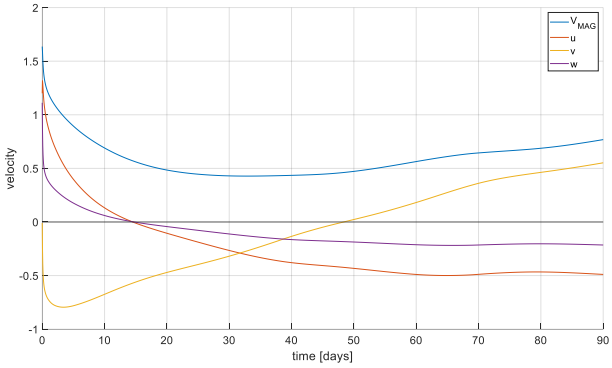

As shown in the picture, the minimum velocity zone is contextual to the WSB inception.

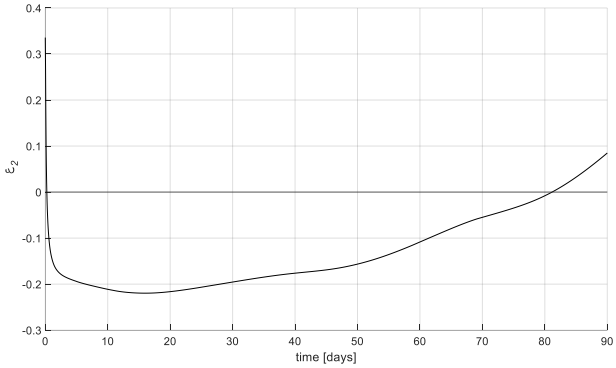

With a significantly shorter mission duration, in the case of ballistic escape without gravity assist, at the instant the trajectory energy changes sign there is no difference in terms of exit velocity from the sphere of influence compared to the case with gravity assist.

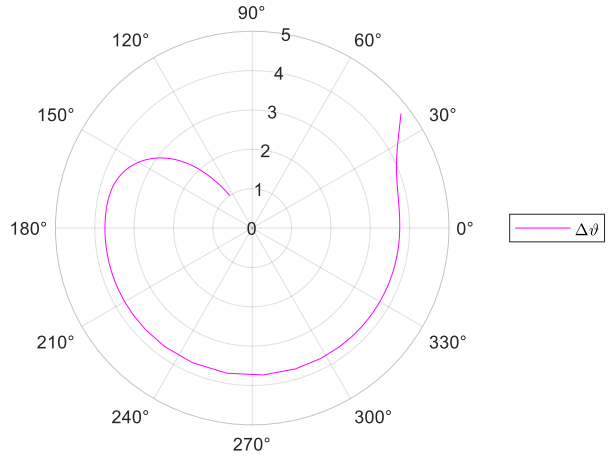

Again, it is clear that it is the solar influence that is the determinant between escape and capture. With a perturbation peak between 0 and 30 degrees, the fourth body determines the escape trajectory of the spacecraft.

7. Conclusions

In conclusion of this study, it becomes evident that the concept of the WSB, even though it originates within the framework of the three-body model, holds

significant practical relevance within a more complex, comprehensive, and reliable physical system. This underscores the versatility and applicability of the WSB concept beyond its original theoretical context.

There remain open avenues for future research, particularly in exploring the influence of the third body over the course of a solar month (rather than a lunar month). This presents an intriguing opportunity to investigate the dynamic effects of the third body across a yearly time span. Such investigations could shed light on novel insights and patterns within the celestial system, offering a fresh perspective on long-term orbital dynamics.

As we continue to advance our understanding of celestial mechanics and orbital dynamics, the WSB concept serves as a valuable tool for unraveling the intricacies of complex systems. It not only enriches our theoretical foundation but also contributes to practical applications within space exploration and mission planning.

References

List of references

[1] Belbruno, Edward & Gidea, Marian & Topputo, Francesco. (2010). Weak Stability Boundary and Invariant Manifolds. SIAM J. Applied Dynamical Systems. 9. 1061-1089. 10.1137/090780638.

[2] Szebehely, V., Chapter 1 - Description of the Restricted Problem, Editor(s): Szebehely, V., Theory of Orbit, Academic Press, 1967, Pages 7-41, ISBN 9780123957320, https://doi.org/10.1016/B978-0-12-395732-0.50007-

[3] Francesco Topputo, Edward Belbruno, Marian Gidea, Resonant motion, ballistic escape, and their applications in astrodynamics, Advances in Space Research, Volume 42, Issue 8, 2008, Pages 1318-1329, ISSN 0273-1177, https://doi.org/10.1016/j.asr.2008.01.017.

[4] Jerry E. White Roger R. Bate Donald D. Mueller. Fundamentals of astrodynamics. 1st ed. Dover Publications, 1971. isbn: 9780486600611; 0486600610

[5] L. Mascolo. «Low-Thrust Optimal Escape Trajectories from Lagrangian Points and Quasi-Periodic Orbits in a High-Fidelity Model». Doctoral Thesis. Torino: Politecnico di Torino, 2023.

[6] Mascolo, L.; Casalino, L. Optimal Escape from Sun-Earth and Earth-Moon L2 with Electric Propulsion. Aerospace 2022, 9, 186. https://doi.org/10.3390/aerospace9040186

[7] J. Fossen. «Analysis of the porkchop plot considering eccentric and inclined planetary orbits». MSc Thesis. Milano: Politecnico di Milano, 2022.

[8] F. Mazzeo. «Utilizzo di algoritmi genetici per ottimizzazioni di trasferimenti interplanetari a bassa spinta ». MSc Thesis. Pisa: Università Degli Studi di Pisa, 2008.